Journal of Molecular Structure 1229 (2021) 129836

Contents lists available at ScienceDirect

Journal of Molecular Structure

journal homepage: www.elsevier.com/locate/molstr

The supramolecular behavior and molecular recognition of adeninium cations on anionic hydrogen selenite/diselenite frameworks: A structural and theoretical analysis

Radhwane Takouachet[a], Rim Benali-Cherif[a,*], El-Eulmi Bendeif[b], Christian Jelsch[b], Fatima Yahia Cherif[c], Ali Rahmouni[c], Nourredine Benali-Cherif[d]

[a] Laboratoire des Structures, Propriétés et Interactions Interatomiques, Université Abbes Laghrour-Khenchela, Khenchela, 40000, Algeria
[b] Université de Lorraine, CNRS, CRM2, F-54000 Nancy, France
[c] Laboratoire de Modélisation et de Méthodes de Calcul, University of Saida Dr. Moulay Tahar, Saida, Algeria
[d] Académie Algérienne des Sciences et de la Technologie (AAST) Algiers. Algeria

ARTICLE INFO

Article history:
Received 7 September 2020
Revised 7 December 2020
Accepted 23 December 2020
Available online 27 December 2020

Keywords:
Adeninium hybrid compounds
Charge transfer
Aromatic stacking interactions
Supramolecular synthons
Intermolecular interactions
DFT

ABSTRACT

In this paper, we report preparation and structure determination of two new adeninium-based hybrid compounds formed with selenious acid: adeninium hydrogen diselenite (**I**) and adeninium hydrogen selenite (**II**). Single crystals of (**I**) and (**II**) were obtained by slow evaporation and their X-ray structures are reported coupled with a quantum chemical density functional theory (DFT) studies. In the atomic arrangement, the different entities are held together through N/O—H···O, N—H···N and C—H···N/O hydrogen bonds on the Watson−Crick, Hoogsteen and sugar sites. Their overall three-dimensional architectures are mostly controlled by electrostatic interactions between the inorganic anion and organic cation frameworks and by hydrogen bonding. Furthermore, the crystal structures of (**I**) and (**II**) contain supramolecular homo and heterosynthons which are present in most similar structures. The similarities and subtle differences of the intermolecular interactions in the two crystal structures have been investigated and discussed using Hirshfeld surface analysis, fingerprint plots, and contact enrichment. The theoretical results are in good relation with the experimental structural analysis and confirm that the charge transfer occurs from inorganic anions to organic cations.

1. Introduction

The ability of small molecules to interact with DNA via an intercalative, groove-binding or electrostatic mode has led to the development of many novel anticancer [1-3] and antimicrobial agents [4]. In this context, nucleobases are key structure directing agents due to their rich and diverse combination of hydrogen bond donor and acceptor positions. Their propensity to self-assemble through hydrogen-bonding interactions has led to a plethora of supramolecular structures. As a significant nucleobase of DNA, adenine is an important naturally occurring nitrogen heterocycle present in nucleic acids. Owing to its unique biological activity and multiple supramolecular interaction, adenine has been extensively studied in varieties of fields such as pharmacology [5-7] and organic functional materials [8]. Recently, adenine has attracted many researchers to study its application as a novel hole-injection layer of OLEDs [9-11]. In addition, interesting adeninium-based organic-inorganic materials have been studied and developed for optoelectronic structures [12]. Moreover, in the past ten years, categories of similar adeninium hybrid compounds have achieved great progresses due to their potential application in the next generation of thin-film solar cell [13,14]. The different properties mentioned above are fundamentally correlated to the structural organizations and to the various intermolecular interactions that govern them. Thereby, understanding the influence of these interactions on the structural properties will be a critical step for the systematic design of functional materials with desired properties. From the structural point of view, adenine can forms crystalline salts in which the adeninium cation can adopt a variety of tautomeric forms. A combined theoretical and experimental study placed the relative stability of the adeninium tautomers in their ground state as 1H,9H > 3H,7H > 3H,9H ≫ 7H,9H > 1H,7H [15] (Fig. 1). Indeed, our careful research on the Cambridge Structural Database (CSD, ConQuest Version 2.0.5, 2020) [16] for crystal structures containing adeninium tautomers results in 96 hits, 66 of them contain

* Corresponding author.
E-mail address: rym_46@hotmail.com (R. Benali-Cherif).

https://doi.org/10.1016/j.molstruc.2020.129836
0022-2860/

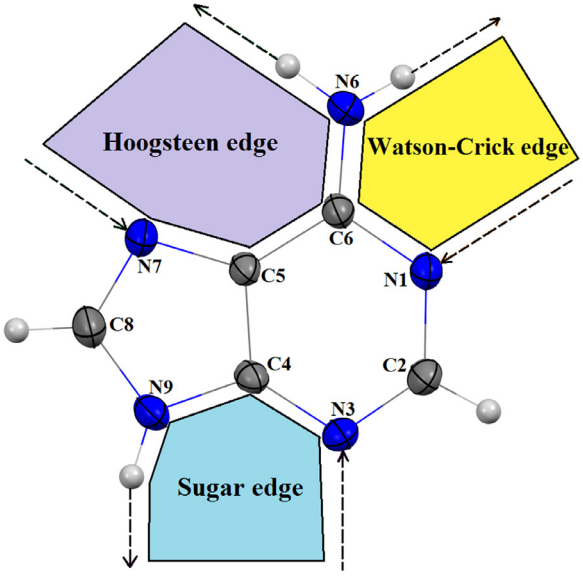

Fig. 1. Adenine structure showing the numbering scheme and characterized by three pairing edges: Watson–Crick, Hoogsteen and sugar.

the 1H,9H tautomer. Therefore, this tautomer is present in almost all the molecular adeninium compounds [17].

The title compounds belong to a series of new selenite-adeninium hybrid materials synthesized in order to study their potentially and interesting optical and dielectric properties [18,19]. Selenite compounds are particularly interesting due to the fact that they often exhibit antioxidant, ferro- or antiferroelectric properties, anti-inflammatory, analgesic and anti-microbial activities, and structural phase transitions [20-24]. In addition, the interest devoted to these compounds is based on the fact that they consist of structurally interesting substances, in which the hydrogen bonds play a very important role [25], and also because a number of them exhibit non-linear optical properties [26].

Having the motivations stated above, we report in this paper the first compound (**I**) based on the hydrogen diselenite anion. According to the CSD data base (CSD, ConQuest Version 2.0.5, 2020) [16] no compound based on this anion has been reported so far, while only two compounds based on diselenites are known (CSD refcodes: AHOYAX and TUYMUV). The second compound (**II**) described in this paper is the sixteenth based on the hydrogen selenite anion, only fifteen hybrid compounds based on this anion have been reported in the CSD.

The two adeninium based organic-inorganic hybrid compounds (**I**) and (**II**) were characterized by single-crystal XRD studies, and a well detailed structural study was illustrated. The graph-set descriptors of the intra- and intermolecular hydrogen bonding interactions stabilizing the two compounds were also discussed. To better understand the contribution of different intermolecular interactions to the supramolecular assembly, Hirshfeld surface analysis was performed. In addition, this work was complemented by DFT calculations to evaluate the charge transfer phenomenon observed in such molecular materials.

2. Experimental

2.1. Chemical preparation

All starting materials were purchased from Sigma-Aldrich and used without any further purification. The crystals of the two compounds (**I**) and (**II**) were obtained by the same chemical reaction and were collected from the same patch. Equi-millimolar amounts of the two starting materials (approximately 1 mmol), adenine and the selenious acid, were dissolved in water (25 mL). After continuously stirring for 1 h, the resultant solution allowed to evaporate at room temperature. Crystals of $[(C_5H_6N_5)^+.(HSe_2O_5)^-]$ (**I**) of brown prismatic shape and of $[(C_5H_6N_5)^+.(HSeO_3)^-]$ (**II**) of pink needle shape were isolated after five weeks. The two types of crystals were manually separated and weighed, the weight ratio $\frac{(\mathbf{I})}{(\mathbf{II})}$ is 0.28. The selected single crystals of (**I**) and (**II**) were subjected to X-ray diffraction analysis.

2.2. Single crystal X-ray diffraction and structure refinement details

The single crystal diffraction measurements were performed on a Bruker APEX II and Nonius KappaCCD diffractometers for (**I**) and (**II**) respectively equipped with a CCD area detector with a graphite monochromatized MoKα radiation, λ = 0.71073 Å. Crystal data, data collection and structure refinement details of (**I**) and (**II**) are summarized in Table 1. The structures were solved in the space groups $P2_1/a$ for (**I**) and $P2_1/c$ for (**II**) by direct methods using the program SIR2014 [27], and successive Fourier difference syntheses, and were refined against F^2 by weighted full-matrix least squares methods including all reflections with SHELXL-2018 program [28]. All calculations were carried out using WingX software package [29]. Structural representations were drawn using Mercury [30]. All absorption corrections were performed with the REFDELF program [31]. All non-H atoms were refined anisotropically. For both compounds all hydrogen atoms were located in difference density Fourier maps. The structures with H atom positions shifted to average bond lengths from neutron diffraction using Mercury CSD 2.0 [30] were used for the geometrical analysis.

2.3. Hirshfeld surface analyses

The fingerprint plots of contacts were generated with the CrystalExplorer3.1 software [32]. The analysis of contact types and their enrichment were computed with the MoProViewer program [33]. In order to obtain integral Hirshfeld surfaces around the cation and the anion, they were computed around an ensemble of two moieties which are not in contact with each other in the crystal. As the Hc hydrogen atoms bound to carbon are less charged than the Ho/n atoms bound to oxygen or nitrogen, the two atom types have different interaction propensities and were treated separately.

2.4. DFT calculations

The energies and electronic properties were calculated using the X-ray crystal structure with H-X bond length elongated to standard neutron diffraction values. The calculations were carried out on two possibilities of asymmetric units and under periodic boundary conditions (PBC) for (**I**) and (**II**) at DFT level. The asymetric units are noted **I-1, I-2, II-1** and **II-2** and showed in Figure. S3. The hybride functional B3LYP [34] and 6–31 G (d, p) basis sets [35] have been used. From the literature, it is well known that B3LYP functional can give structural properties in good agreement with experimental one [36,37]. Gaussian 09 was used for all calculations [38]. The visualization and analysis of the calculated results were done using Gaussview [39] and GaussSum [40] softwares.

3. Results and discussion

3.1. Description of crystal structure

Structural data for (**I**) and (**II**) are given in Table 1. For comparison between adeninium cations in the two structures, bond

Table 1
Main crystallographic data and structure refinement details for **(I)** and **(II)**.

Crystal data	(I)	(II)
Empirical Formula	C_5 H_7 N_5 O_5 Se_2	C_5 H_7 N_5 O_3 Se
Molecular weight (g/mol)	375.08	264.12
Diffractometer,	Bruker APEX-II CCD	Nonius KappaCCD
Radiation type	Mo Kα (λ=0.71073 Å)	Mo Kα (λ=0.71073 Å)
T (K)	293(2)	293(2)
Calculated density (Mg/m^3)	2.410	2.034
Crystal system	Monoclinic	Monoclinic
Space group	*P* $2_1/c$	*P* $2_1/a$
a (Å)	6.2851 (3)	6.5612 (2)
b (Å)	21.0046 (2)	12.7621 (2)
c (Å)	8.1402 (2)	10.4529 (3)
β (°)	105.838 (1)	99.846 (3)
V (Å^3)	1033.84 (6)	862.38 (4)
Z	4	4
μ (mm^{-1})	7.17	4.35
Crystal size (mm)	0.15 × 0.10 × 0.08	0.15 × 0.05 × 0.04
No. of measured, independent and observed [**I** > 2σ(***I***)] reflections	19,963, 5116 3995	13,979, 2507 1940
R$_{(int)}$[a] Refinement	0.044	0.085
$R[F^2 > 2\sigma(F^2)]$[b], w$R(F^2)$[c], S[d]	0.033, 0.087, 1.07	0.034, 0.091, 1.03
No. of unique reflections	5116	2507
No. of parameters	154	127
$\Delta\rho_{max}$, $\Delta\rho_{min}$ (e Å^{-3})	1.16, −0.88	0.55, −0.71

[a] $R(\text{int}) = \Sigma(F_o^2 - <F_o^2>)] / \Sigma(F_o^2)$.
[b] $R_1 = \Sigma||F_o|-|F_c|| / \Sigma|F_o|$.
[c] $wR_2 = \{[\Sigma w(F_o^2-F_c^2)^2] / [\Sigma w(F_o^2)^2]\}^{1/2}$.
[d] Goodness-of-fit $S = [\Sigma w(F_o^2 - F_c^2)^2/(n-p)]^{1/2}$, where n is the number of reflections and p the number of parameters.

Table 2
Selected structural parameters, bond lengths (Å) and bond angles (°) of adeninium cations in (**I**) and (**II**).

		(I)	(II)
	Bond lengths (Å)		
	N6—C6	1.312 (3)	1.310 (3)
Pyrazine	N1—C6	1.366 (3)	1.362 (3)
Pyrazine	C6—C5	1.406 (3)	1.412 (3)
Pyrazine	N3—C4	1.359 (3)	1.363 (3)
Pyrazine	N3—C2	1.304 (3)	1.305 (3)
Pyrazine	N1—C2	1.358 (3)	1.357 (3)
Imidazole	C4—C5	1.384 (3)	1.379 (3)
Imidazole	N7—C5	1.380 (2)	1.378 (3)
Imidazole	N7—C8	1.314 (3)	1.312 (4)
Imidazole	N9—C8	1.367 (3)	1.361 (4)
Imidazole	N9—C4	1.361 (3)	1.357 (3)
	Bond angles (°)		
Pyrazine	C2—N1—C6	123.74 (18)	123.6 (2)
Pyrazine	N1—C6—C5	113.69 (18)	114.0 (2)
Pyrazine	C4—C5—C6	118.03 (18)	118.0 (2)
Pyrazine	N3—C4—C5	127.08 (19)	126.6 (2)
Pyrazine	C2—N3—C4	112.29 (19)	112.7 (2)
Pyrazine	N3—C2—N1	125.21 (19)	125.0 (2)
Imidazole	N7—C5—C4	110.76 (18)	111.0 (2)
Imidazole	N9—C4—C5	105.57 (18)	105.9 (2)
Imidazole	C8—N7—C5	103.93 (18)	103.0 (2)
Imidazole	N7—C8—N9	113.18 (19)	114.3 (2)
Imidazole	C4—N9—C8	106.56 (18)	105.8 (2)

Table 3
Geometric parameters of the O/N—H•••O/N hydrogen bonds parameters (Å, °).

D—H•••*A*	*D*—H (Å)	H•••*A* (Å)	*D*•••*A* (Å)	*D*—H•••*A*(°)
Compound (I)				
O1—H1•••O3^{i}	0.99	1.64	2.621 (2)	166
C2—H2•••O2^{i}	1.08	2.27	3.351 (3)	170
N6—H66*N*•••O3^{ii}	1.01	1.86	2.878 (2)	172
N1—H1*N*•••O4^{ii}	1.01	1.65	2.635 (2)	161
N6—H6*N*•••N7^{iii}	1.01	1.91	2.909 (3)	167
N9—H9*N*•••N3^{iv}	1.01	1.92	2.909 (3)	163
Compound (II)				
N6—H66*N*•••N3^{i}	1.01	1.86	2.854 (3)	164
N6—H6*N*•••O2^{ii}	1.01	1.85	2.771 (3)	149
N1—H1*N*•••O3	1.01	1.67	2.670 (3)	168
O1—H1•••O3^{iii}	0.99	1.75	2.708 (3)	161
N9—H9*N*•••O2^{iv}	1.01	1.73	2.725 (3)	166

Symmetry codes for (**I**): (**i**) $x+1, y, z$; (**ii**) $x+1, y, z+1$; (**iii**) $-x, -y, -z+1$; (**iv**) $-x+1, -y, -z$; Symmetry codes for (**II**): (**i**) $-x+½, y-½, -z$; (**ii**) $-x+1, -y+1, -z+1$; (**iii**) $x+½, -y+3/2, z$; (**iv**) $x-½, -y+3/2, z-1$.

lengths and internal angles of pyrazine and imidazole rings are collected in Table 2. Both new crystalline compounds are stabilized by several hydrogen bonds that are summarized in Table 3.

The new organic-inorganic hybrid compounds (**I**) and (**II**), were prepared from adenine and selenious acid. Our initial products were selected based on the multifold noncovalent interactions of adenine through the Watson–Crick, Hoogsteen and sugar-face N atoms or N—H bonds, with small molecules. Adenine takes part in crystalline structures via its multiple functional groups, namely a five membered imidazole ring fused to a six-membered pyrazine ring, and an external amine group. The N atoms of the adenine molecule are assigned in Fig. 1 according to IUBMB nomenclature to facilitate the description of the structure analysis.

3.1.1. Crystal structure of adeninium hydrogen diselenite (I)

The crystal structure of (**I**) with the formula $(C_5H_6N_5)^+.(HSe_2O_5)^-$ belongs to the monoclinic $P2_1/c$ space group. The asymmetric unit consists of one adeninium cation and one hydrogen diselenite anion. Structural analysis by X-ray diffraction has shown that proton transfer has taken place and the adeninium cation is in the common 1H,9H tautomeric form (Fig. 2). The protonation process is confirmed by the larger endocyclic angle around the protonated nitrogen site N1 on the

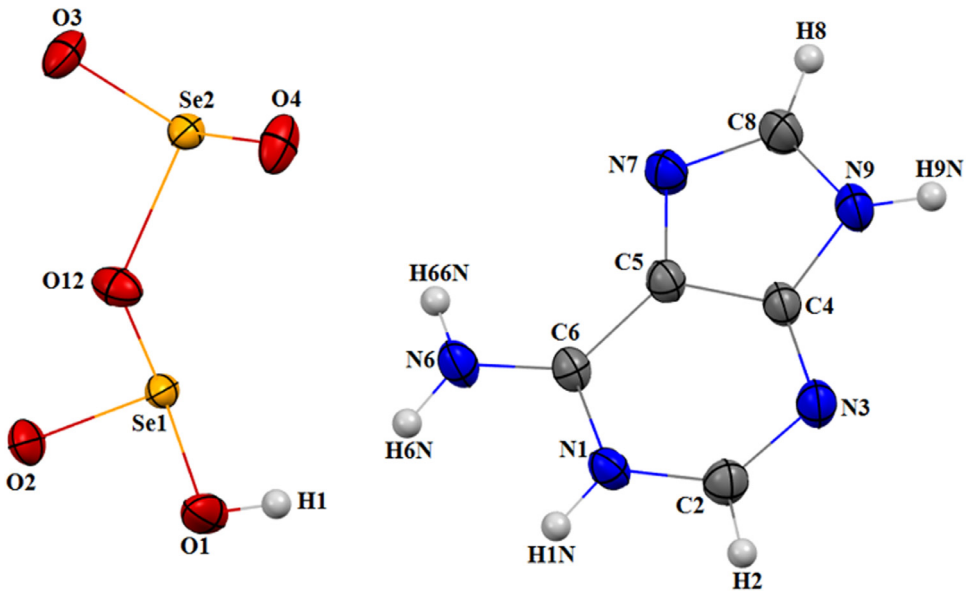

Fig. 2. The asymmetric unit of adeninium hydrogen diselenite (**I**) showing the atom-numbering scheme. Displacement ellipsoids are drawn at the 50% probability level.

Watson–Crick face. Hence, the internal angle at N1 [C6—N1—C2 = 123.74 (18)°] is increased from the mean reported value of 119.8° for unprotonated adenine [41]. This protonation enlarges the C—N—C angle by +3.94° (see Table 2). As in most purine derivatives, the adeninium base is close to flatness and the pyrimidine and imidazole rings are slightly folded around the C4—C5 bond by 1.83° Examining the interatomic distances and angles of the adeninium cations in (**I**) shows that the majority of the bond lengths and angles found in (**I**) are fairly similar to those in the adeninium cations protonated at the N1 and N9 atoms [12, 42-48].

The hydrogen diselenite anion $(HSe_2O_5)^-$ is formed from two selenious acid groups (H_2SeO_3), that have a common oxygen atom as a bridge between two selenium atoms. This bridged selenium—oxygen distance is elongated with bond lengths of 1.8148 (14) Å and 1.8281 (14) Å for Se1—O12 and Se2—O12 respectively. The first O3—Se2—O4 group shows two short Se—O bonds (Se2—O3 = 1.6619 (14) Å and Se2—O4 = 1.6569 (15) Å), whereas the second group O1—Se1—O2 has only one short bond length [Se1—O2 =1.6186 (15) Å]. One notes that the Se1—O1 bond is significantly longer (1.7508 (16) Å) indicating that the hydrogen atom (H1) is connected to the O1 atom causing elongation of the selenium—oxygen bond (Table S1). It is noteworthy that this is the first time that hydrogen diselenite anion has been observed in a crystalline form [16].

The structure of (**I**) can be described as the succession of cationic layers sandwiched between parallel bilayers of hydrogen diselenite anions developing along the **b**-axis (Fig. 3).

In (**I**), the adeninium cations are arranged into; a centrosymmetric homosynthon $R_2^2(10)$ ring motifs [49] through a double N6—H6N···N7^{iii} interaction that mimics the Hoogsteen pattern and a centrosymmetric homosynthon $R_2^2(8)$ ring motif via two N9—H9N···N3^{iv} interactions that mimics the sugar pattern (Fig. 4) [50-51]. The whole Watson–Crick edge and atom C8 from the Hoogsteen edge are interacting with hydrogen diselenite anions (Fig. 4).

Adeninium base pairs are stacked together through an inversion center and the interplanar distance is 3.361(14) Å (Fig. 5a) to form planar ribbons parallel to the [101] direction. The borders of these organic ribbons are framed by hydrogen diselenite ions (Fig. 4). Each adeninium cations dimer is interacting with four different hydrogen diselenite anions through N6—H66N···O3^{ii} ($d_{D...A}$ = 2.878 (2) Å) and N1—H1N···O4^{ii} ($d_{D...A}$ = 2.635 (2) Å) hydrogen bonds, giving rise to an $R_2^2(8)$ heterosynthon on the Watson–Crick edge [52-55], and through weak and non-conventional C8—H8···O12 and C2—H2···O2^{i} intermolecular interactions thereby forming $R_3^3(10)$ and $R_4^3(11)$ ring motifs (Fig. 4). To the best of our knowledge, these three supramolecular features have been observed in only one similar compounds, the adeninium dichromate [56]. Moreover, the cationic molecules stack together to form two-dimensional organic layers as shown in Fig. 3.

Additionally, the oxygen O1—H1 group of the selenite anion is hydrogen bond donor to the O3 oxygen of translated neighbour (X + 1,Y,Z) to form a chain of formula $(HSe_2O_5)_n^{n-}$ along the **a**-axis. This chain is described by the $C_1^1(6)$ graph set via the O1—H1···O3^{i} hydrogen bond [$d_{D...A}$ = O1—H1···O3= 2.621 (2) Å] (Fig. 4). According to the geometrical parameters (Table 3), the O1—H1···O3 and the N1—H1N···O4 hydrogen bonds seem to be the strongest hydrogen bonds in the 3D molecular packing of (**I**). The electrostatic attractive contact d = 2.77 Å between atoms Se1 and O4 (symmetry X, ½-Y, ½+Z) is much shorter than the sum of van der Waals radii 1.90+1.52 = 3.42 Å. There are five other Se···O contacts in crystal I which are all shorter than the sum of van der Waals radii (in the range 2.97- 3.21 Å).

Moreover, anions molecules play an important role in the three-dimensional network. They maintain cohesion in the organic ribbons layers, as the four oxygen atoms out of five are involved in hydrogen bonding as acceptors, while the OH group is hydrogen bond donor (Table 3 and Fig. 5b). Furthermore, this OH oxygen atom O1 exhibits an electrostatic contacts with the π –hole of C2 carbon atom of the pyrimidine ring, resulting in a very short O1—$C2_{ring}$ contact, the distance of O1 to the ring plane is only 2.94(2) Å. This cation···$O^{\delta-}$ supramolecular association contributes to the stabilization of the molecular structure of (**I**) (Fig. 5b). This oxygen atom, potential acceptor, is indeed not involved in any hydrogen bond.

3.1.2. Crystal structure of adeninium hydrogen selenite (II)

The crystal structure of (**II**) with the formula $(C_5H_6N_5)^+.(HSeO_3)^-$ has an asymmetric unit containing one adeninium cation and one hydrogen selenite anion held together by hydrogen-bonding and electrostatic interactions (Fig. 6). As observed in (**I**), the proton is also transferred from the selenious acid

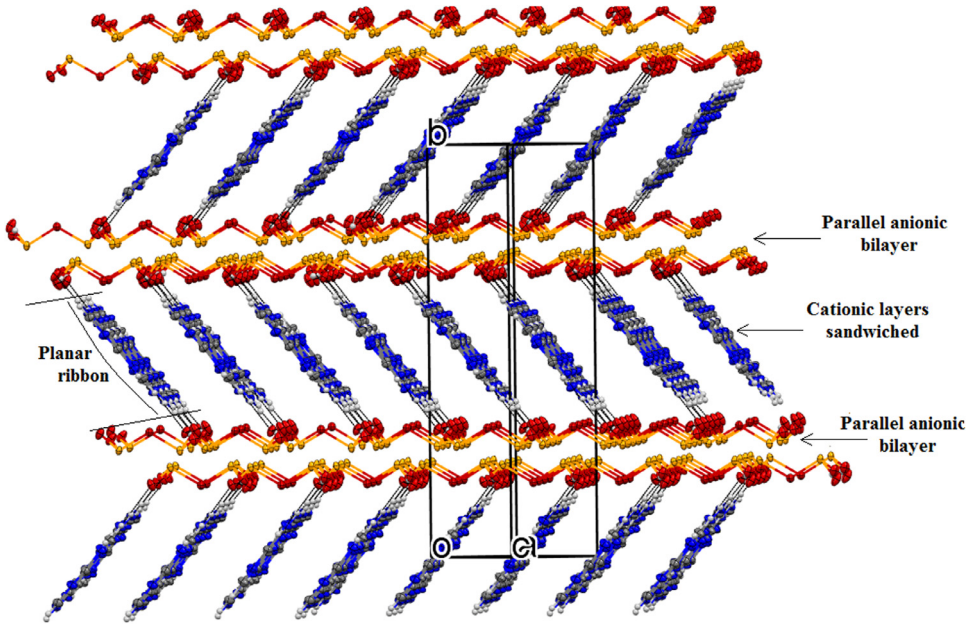

Fig. 3. A view of the crystal packing of (**I**) showing the stacking of adeninium cations and hydrogen diselenite anions.

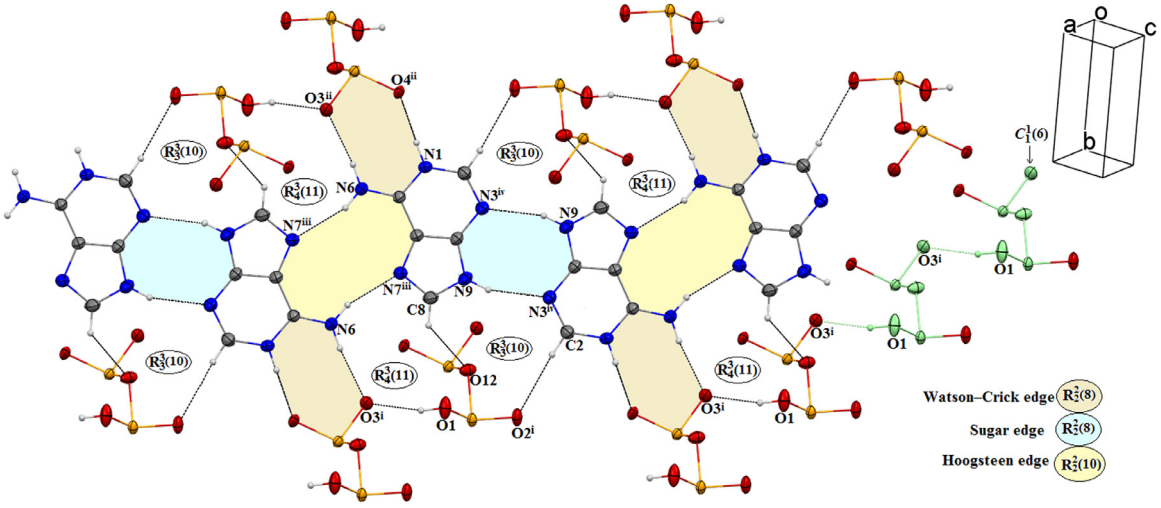

Fig. 4. Part of packing diagram of (**I**) showing the 1D cationic ribbons framed by hydrogen diselenite anions and illustrating the formation of $R_2^2(8)$, $R_2^2(10)$, $R_4^3(11)$ and $R_3^3(10)$ ring motifs and $C_1^1(6)$ infinite chain. Dashed lines indicate N/O–H•••O, N–H•••N and C–H•••O hydrogen-bonding interactions.

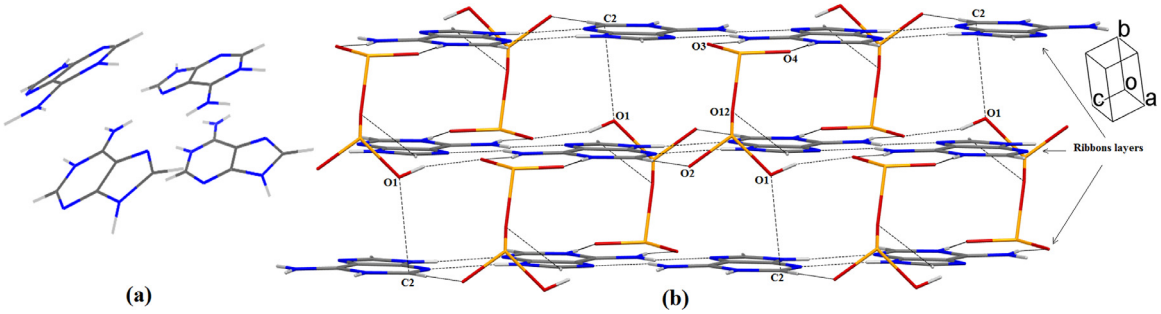

Fig. 5. A fragment of the (**I**) crystal structure, (**a**) Crystallographic autostereogram of the stacking interaction between adeninium cations contributing to the maintenance of the organic layers. The **a** axis corresponds to the horizontal direction. (**b**) Electrostatic interaction between the O1 atom and the adeninium cation. Intermolecular interactions are shown as black dashed lines.

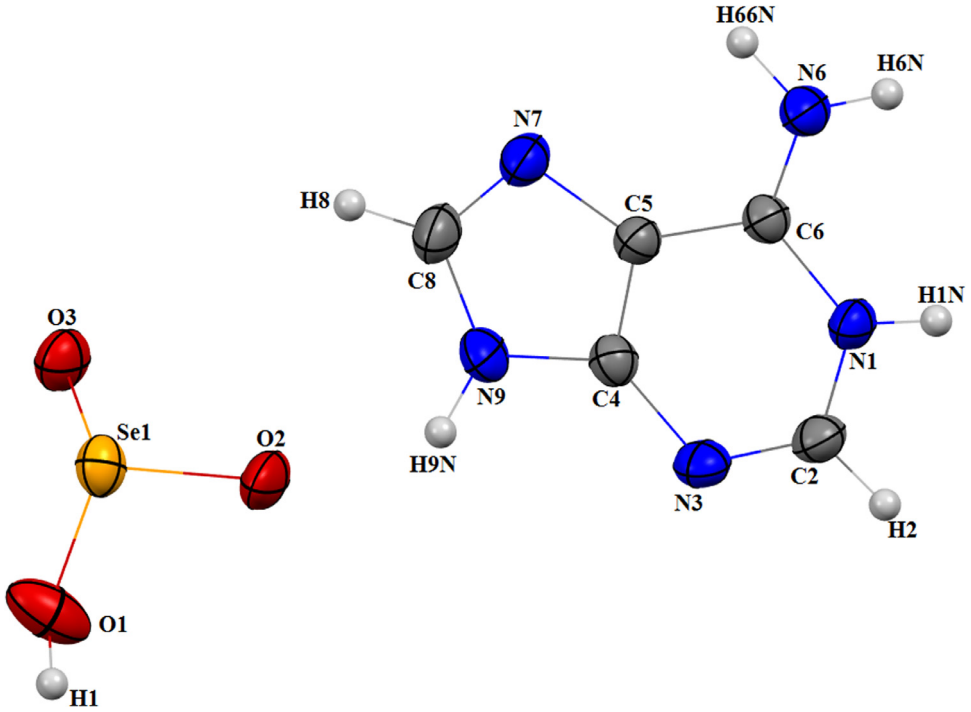

Fig. 6. The asymmetric unit of adeninium hydrogen selenite (**II**) showing the atom-numbering scheme. Displacement ellipsoids are drawn at the 50% probability level.

to the aromatic nitrogen (N1). This proton transfer enlarges the C2—N1—C6 endocyclic angle by +3.8° (see Table 2) in comparison to the unprotonated adenine [41]. The geometrical features of the adeninium cations are similar to those previously described in (**I**). Indeed, the adeninium cations exhibit the usual 1H, 9H tautomeric form and are nearly planar, with an r.m.s. deviation of 0.002 Å from the (C6/N1/C2/N3/C4–C5/N7/C8/N9) least-squares plane. The maximum deviations (0.0230(2) Å) from this mean plane was observed for the N1 atom.

Inspection of the anion bond distances shows the presence of two short and one long Se—O bond, clearly indicating the protonation of O1 atom [Se—O1= 1.773(2) Å], whereas both O2 and O3 atoms are bare [Se—O2= 1.638(2) Å and Se—O3= 1.673(2) Å]. This observation confirms that one of the protons was transferred from the selenious acid to the adenine molecule. The hydrogen selenite anion $(HSeO_3)^-$forms a trigonal prism with the three oxygen atoms and one selenium atom at the apexes. The geometrical features of the inorganic anions $(HSeO_3)^-$ (Table S1) are typical and are in good agreement with those observed in similar compounds [57].

The structure is built up from tunnels, prolonged along the **b**-axis at (½, *y*, ½) and (0, *y*, 1). These tunnels are formed by the intersections of two types of chains. The first one is the combination of the inorganic hydrogen selenite anions and the second is constituted by the protonated adeninium organic groups (Fig. 7a). This type of stacking has been observed in adeninium bis (adeninium) selenate bihydrates [58] and in cytosinium hydrogen selenite [57] compounds.

In (**II**), the 1H,9H-adeninium cations form together a non centrosymmetric Hoogsteen/sugar edge pair with N6—H66N···N3^{i} and C2—H2···N7 interactions thereby generating an $R_2^2(8)$ heterosynthon motif [59] that contains both strong and weak hydrogen bonds. From the variety of bidentate hydrogen-bonded dimers that could be formed by adeninium cations, only this base pair is observed in (**II**). Instead, the Watson–Crick face and atom N9 from the sugar edge are involved in direct interactions with the hydrogen selenite anions.

Adeninium moieties are located in layers parallel to the (**a,b**) plane around $z = n$, with the stacking occurring in the **a** direction. Along the **b**-direction, the base pairs are arranged together into one dimensional cationic ribbons. The ribbon edges are bordered by hydrogen selenite anions which form together a supramolecular homo-synthon dimer assembled with two centro-symmetric related Se1···O3 ionic interactions with Se···O distances of 3.233(2) Å (Fig. 7b). This dimer is further linked to its inversion-related dimer through four hetero-synthons ionic dimers which are formed by means of O1···Se1 electrostatic interactions and O1—H1···O3^{iii} hydrogen bond (Table 3). These six dimers lead to the formation of a hexameric intermolecular interactions network. The hexamers centers are repeated at the middle of the four edges of the **ab** plane (Fig. 8a). Further, the connectivity between these hexamers generates a three-dimensional honeycomb-like inorganic framework (Fig. 8b). The two-dimensional honeycomb-like layers are stacked along the crystallographic **c**-axis (Fig. 8b). The O1 oxygen atom (from the SeOH moiety) does not form any hydrogen bond, but is involved in three long distance H···O electrostatic interactions ($d_{H...O}$ >2.7 Å), the shortest being the Se-O1-H1···O1

Each adeninium cation interacts through its Watson–Crick face (N1 and N6 atoms) with the anionic homosynthon mentioned above through moderates N1—H1N···O3 and N6—H6N···O2^{ii} hydrogen bonds. Due to the interaction with inorganic dimers on one side, and with the inversion-related inorganic dimer on the other side, the N9 atom from the sugar face of adeninium cation is free to establish a N9—H9N···O2^{iv} hydrogen bond to generate an $R_2^2(8)$ motif spread out along the **b**-direction. In addition, another $R_6^6(22)$ ring type is created by the interactions of four adeninium cations with two hydrogen selenite anions (Fig. 7b).

Similarly to (**I**), the cationic ribbons in (**II**) stack together to form two-dimensional layers running in the **a**-direction (Fig. 9). These layers are held together through aromatic stacking interactions established between, one via an inversion centre (d_{planes}= 3.270(4) Å) and one via a 2-fold axis. The distance of the C2···C2 interaction around the 2-fold rotation axis centre is $d_{C2...C2}$ = 3.364 (4) Å. Each adeninium cation forms a total of four aromatic stack-

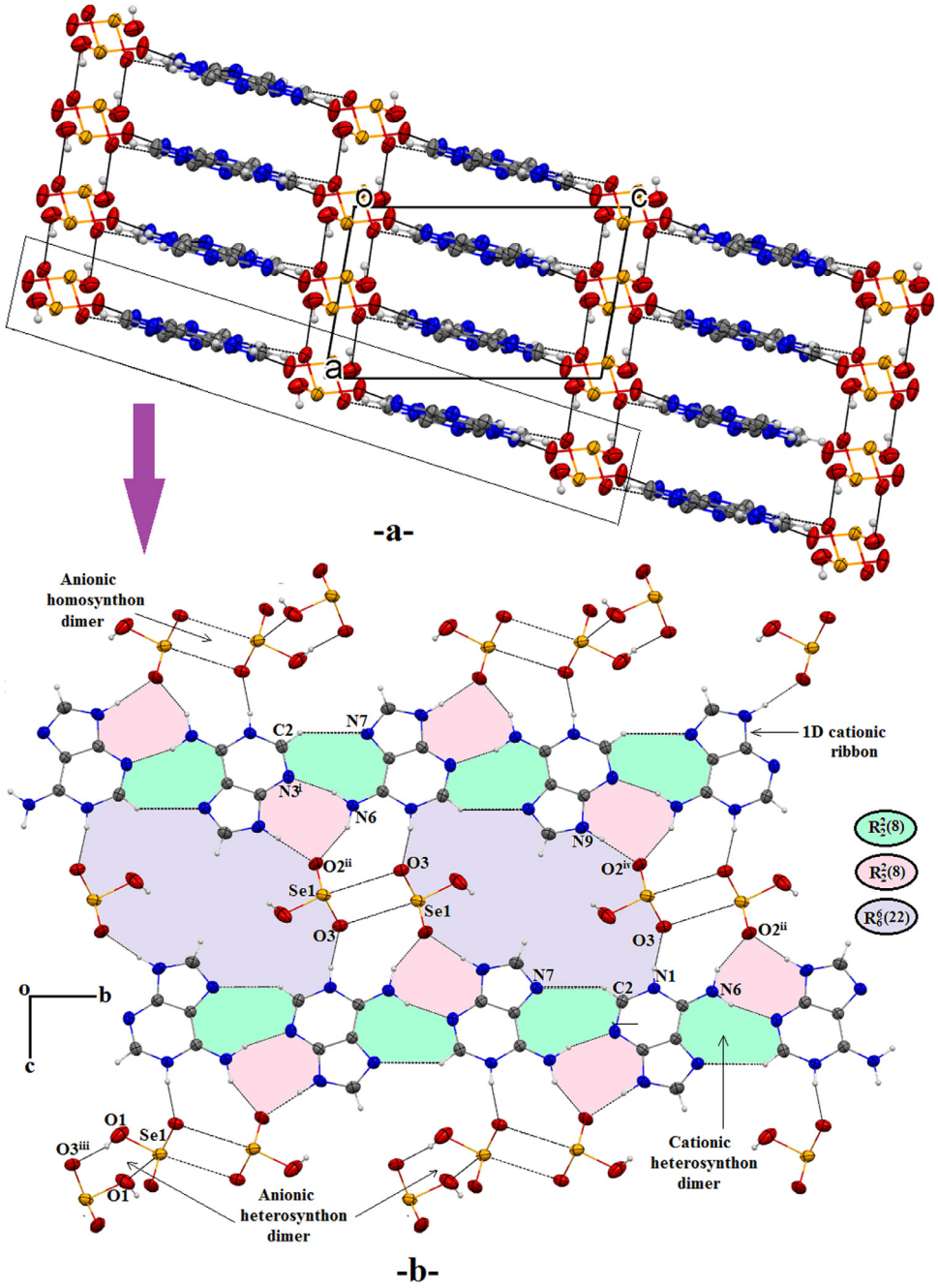

Fig. 7. (**a**) The crystal packing of (**II**) in projection along the **b**-axis, showing the cationic and anionic entities arranged in tunnels. **(b)** A fragment of (**II**) showing the supramolecular synthons and the graph set describing intermolecular interactions.

ing interactions, i.e. two on each side of the moiety (Fig. 9). An energetic analysis of protonated nucleobases/chloride crystal structures [17,60] showed that the organic cations can form metastable base pairs which are stabilized by the surrounding anions. Furthermore, hexamers play an important role in stabilizing the crystal packing, in which each hexamer contribute to bridge three successive ribbons layers via hydrogen bond interactions (Fig. 9)

In summary, in both compounds the adeninium cations adopt the most common 1H, 9H-adeninium tautomer, and their geometrical parameters is almost identical (see Table 2). The configuration of the adeninium cations is comparable to the thirteen adeninium-based organic-inorganic hybrid compounds with the same tautomeric form reported in the CSD [16]. An illustration of this comparison is represented in Fig. 10.

The structural investigation shows that the 1H,9H-adeninium in both crystal structures generate cationic ribbons, where they are formed from centrosymmetric homosynthons in (**I**) and heterosynthons in (**II**). Therefore, the supramolecular homo and heterosynthon motifs are one of the classical motifs frequently observed in similar adenine-based hybrid compounds formed with different oxoanions [61-65].

Moreover, the inspection of hydrogen bonding network in both compounds shows a direct hydrogen-bond interactions between the adeninium cations and the hydrogen (diselenite/selenite) an-

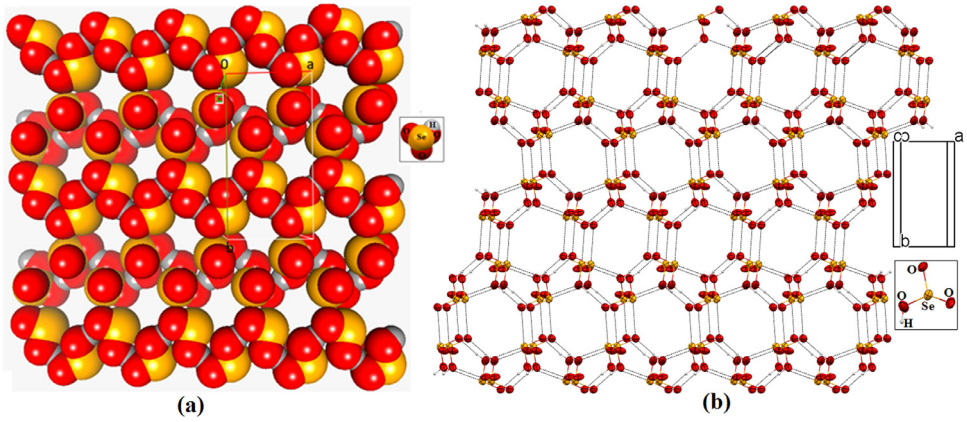

Fig. 8. Molecular packing diagram of hydrogen selenite anions in (**II**) showing honeycomb-like molecular network. (**a**) 2D crystallographic autostereogram and (**b**) 3D view.

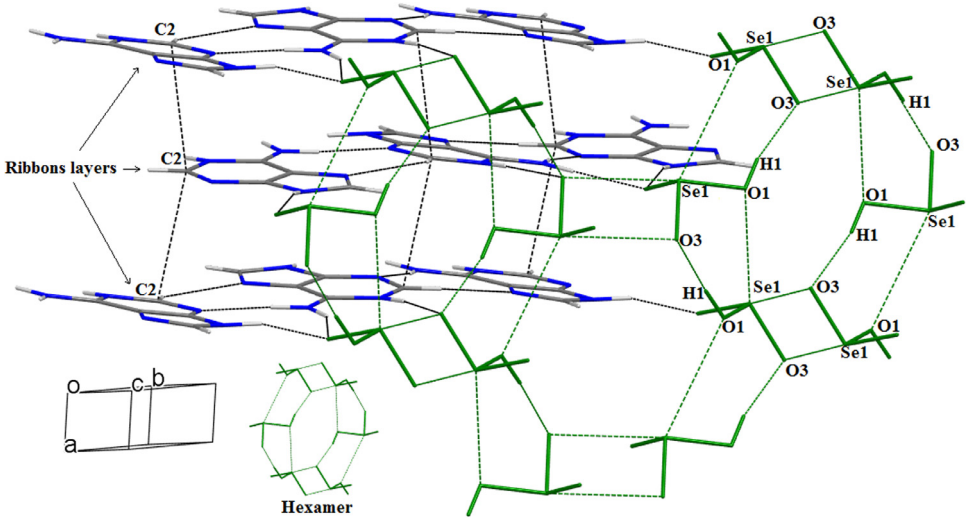

Fig. 9. Three dimensional crystal structure of (**II**) showing the role of selenite hexamers and aromatic stacking in stabilizing the crystal packing.

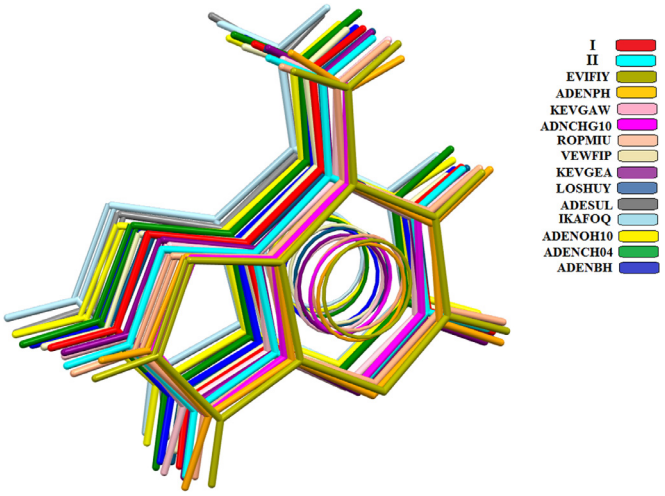

Fig. 10. Comparison of the geometry of adeninium cations in (**I**) and (**II**) with the thirteen 1H, 9H- tautomers of adeninium cations deposited in the CSD with their REFCODE.

ions. In (**II**), the adeninium cations are connected to anions via three N—H···O hydrogen bonds, while in (**I**), the two entities are connected through two N—H···O interactions and two C—H···O weaker hydrogen bonds.

In the molecular packing of the two compounds, anions play an important role in maintaining the three-dimensional network through hydrogen bonds and electrostatic charge-charge interactions. In (**I**) the anions exercise their role in solo while in (**II**) they do it as hexamers.

In addition to the N—H···N and C—H···N hydrogen bonds connecting the purine bases in (**I**) and (**II**), weak stacking interactions are observed between the aromatic rings of the adeninium base in both compounds. It is interesting to note that the molecular arrangement of the adeninium cations in (**I**) is completely different to that observed in (**II**). While in (**II**), an arrangement of parallel cationic layers is found, the organic $(C_5H_5N_6)^+$ adeninium planes in (**I**) take different orientations in the successive organic layers to form a zigzag pattern.

3.2. Hirshfeld surface analysis and contacts enrichment ratio

The intermolecular contact types were computed by Hirshfeld surface analysis in order to evidence which contacts play a major role in the crystal packing stabilization. The enrichment ratio [66] is a powerful descriptor to find which type of contacts are over- or under-represented in the crystal packing. The enrichment

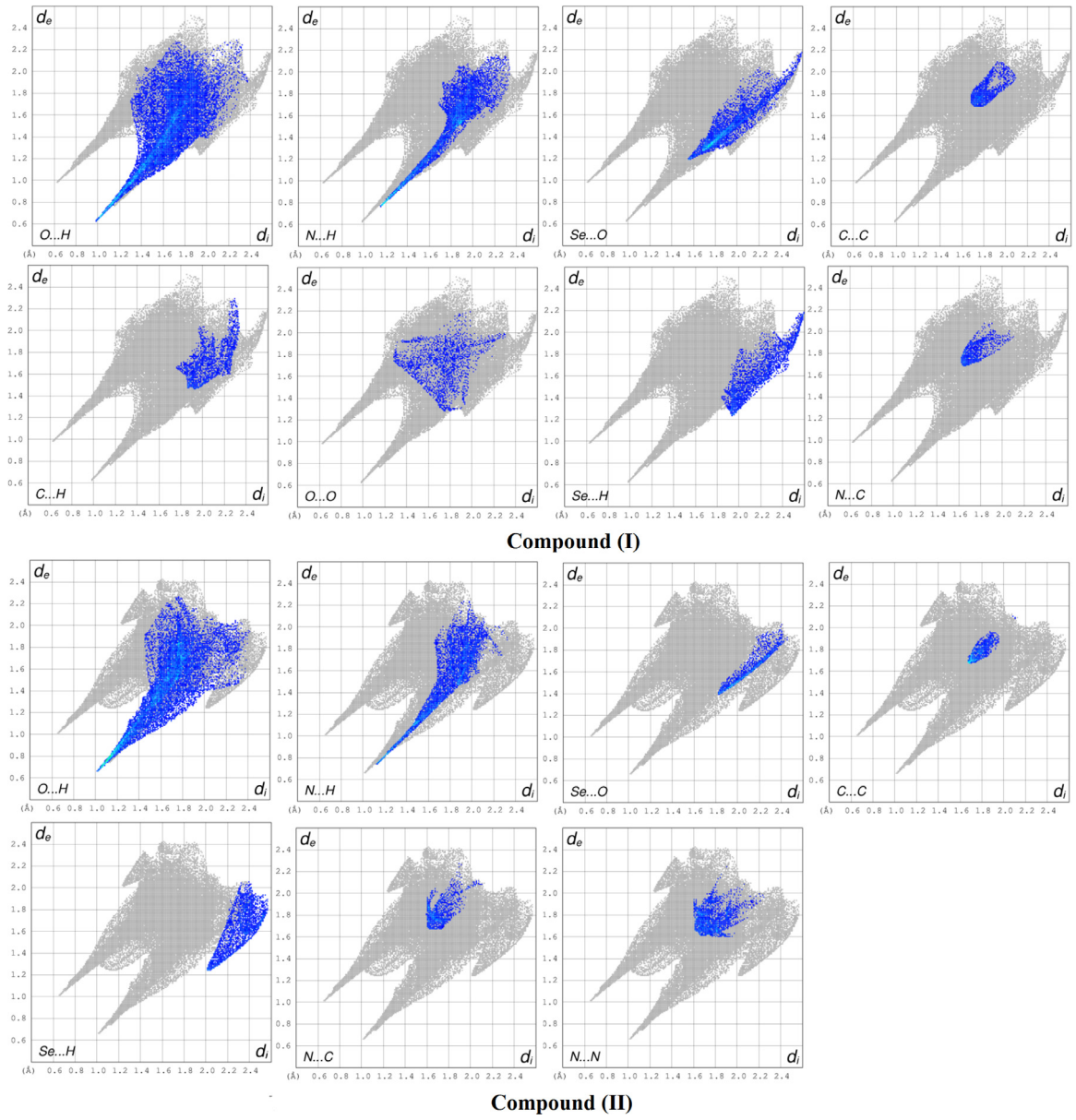

Fig. 11. Fingerprint plots showing the main contacts of the two compounds. Reciprocal contacts were not merged; they can be deduced by symmetry of the plots.

E_{xy} compares the actual contacts C_{xy} and the R_{xy} "random" contacts, computed as if all types of contacts were equi-probable.

The two crystals show globally similar packing trends with alternative layers of anions and cations, which is reflected by the correlation of the contacts types reaching 70% and of the contacts enrichment ratios at 54%. Fig. 12 shows the Hirshfeld interface between the cation and anion layers which are parallel to the (**a,b**) plane. The contact surface of the organic cation layers is constituted by up to 84% of hydrogen atoms (Table.S2). At the layers interface, the contacts of selenium with all atoms of the cation (C, Hc, N) are favoured except those with the positively charged Hn atoms.

Overall, hydrogen occupies the largest proportion of the Hirshfeld surfaces, reaching 28.9% for (**I**) and 34% for (**II**) most of which is constituted by the polar Hn/o type (Table. 4). For both compounds, the major contacts are constituted by strong O···H—N/O and N···H—N hydrogen bonds. The Ho/n···O contacts are enriched (E = 1.46 for (**I**) and E = 2.37 for (**II**)); the difference corresponds to the presence of three strong N—H···O hydrogen bonds in (**II**) and only two in (**I**).

Furthermore, there is a double proportion of Se···O electrostatic interactions in crystal (**I**) compared to compound (**II**), due to the presence of hydrogen diselenite ion in the (**I**) crystal. The Se…O contacts are moderately over-represented in both crystals. Also, the C—H···O weak hydrogen bonds have a higher content and are more enriched in (**I**) than in (**II**). The hydrophobic C···C contacts are limited (below 6%) in the two crystals but are among the most enriched at E_{cc}>1.8 due to stacking between the aromatic pyrazine rings. The C···N and to a lesser extend the N···N contacts are also quite favoured as a consequence of the aromatic stacking.

The fingerprints of both compounds (Fig. 11) exhibit some similarity in the global shape and the contributions of the different

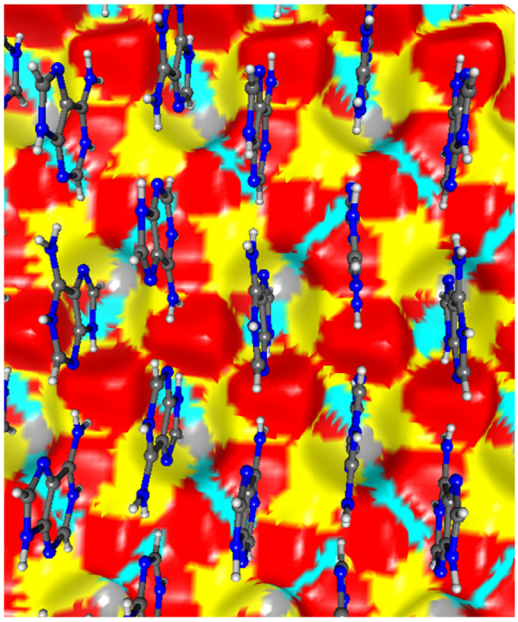

Fig. 12. Crystallographic autostereogram view of Hirshfeld surface at the interface of the organic cations layer (shown in front) and the layer of selenite anions (compound **II**). Surface coloring: red: oxygen, yellow: selenium, light grey: Hc hydrogen, light blue: Ho hydrogen (H–O).

Table 4
Analysis of contacts on the Hirshfeld surface. Reciprocal contacts X…Y and Y…X are merged. The second line shows the chemical content on the surface. The% of contact types between chemical species is given in the next six lines, followed by their enrichment ratios. The major contacts, as well as the most enriched ones, are highlighted in bold characters. The polar Hn/o hydrogens bound to nitrogen or carbon are distinguished from the less charged Hc atoms bound to a carbon atom.

(**I**)	O	N	Ho/n	Se	Hc	C
surf%	23.8	13.4	20.4	18.4	8.5	15.6
O	0.0					
N	2.4	1.8		%	contacts	
Ho/n	**14.9**	**12.4**	0.5			
Se	**15.9**	1.1	5.8	4.6		
Hc	**8.6**	0.4	3.0	2.7	0.0	
C	**7.5**	5.5	4.5	2.3	2.2	4.1
O	0.00					
N	0.38	1.11			enrichment	
Ho/n	**1.46**	**2.36**	0.11			
Se	**1.75**	0.24	0.75	**1.34**		
Hc	**2.06**	0.17	0.86	0.87	0.00	
C	1.01	**1.44**	0.71	0.41	0.87	**1.81**
(**II**)	O	N	Hn/o	Se	Hc	C
%	18.7	15.9	22.6	13.3	11.4	18.1
O	0.0					
N	1.0	3.3		%	contacts	
Hn/o	**21.2**	**6.5**	2.7			
Se	**7.6**	1.5	5.1	1.9		
Hc	5.6	4.7	2.2	**7.0**	0.6	
C	2.8	**10.2**	6.3	2.8	0.9	6.1
O	0.00					
N	0.17	**1.41**			enrichment	
Hn/o	**2.37**	0.92	0.50			
Se	**1.44**	0.36	0.79	0.97		
Hc	**1.35**	**1.43**	0.43	**2.33**	0.54	
C	0.41	**1.91**	0.77	0.56	0.24	**1.98**

types of intermolecular contact. The O···H/H···O contacts can be considered as dominant and appear as a pair of sharp symmetric spikes at short distance. The N···H contacts contribute also secondarily to the spikes. The presence of these long spikes at short intermolecular distances is characteristic of strong O—H···O and N—H···O hydrogen bonds.

3.3. DFT quantum chemical calculations

3.3.1. Frontier molecular orbital analysis

The Frontier molecular orbitals (FMOs) of dimers complexes are imperative parameters for determining the way the monomers molecules interacts. As appear from Fig. 13, the HOMO orbitals of the two compounds are exclusively delocalised on the atoms of anions, when these laters have small contributions in the LUMO orbitals that are mainly located over all adeninium atoms. The LUMO orbitals in the two compounds are dues to the interactions between π-type atomic orbitals. As shown by Fig. 13, the interactions between adeninium and hydrogen diselenite in configuration **I-1** result in lower HOMO energy and higher energy LUMO than their interactions in configuration **I-2**. Consequently the HOMO-LUMO gap of configuration **I-1** is larger than the HOMO-LUMO gap of configuration **I-2**. These constatations with the comparison of total configurations energies let to conclude that the configuration **I-1** is more stable than configuration **I-2**. The same conclusion is made for II. In that case, the configuration **II-2** is more stable than configuration **II-1**. Under periodic bondary conditions, the anion-cation dimers exhibit smaller energy in magnitude than their isolated configurations (Table S4).

The density of state (DOS) and the partial density of state (PDOS) spectrum created by convoluting the molecular orbital using GAUSSIAN curves of unit height and full width at half-maximum of 0.2, demonstrate the number of molecular orbitals and the contributions of adeninium and hydrogen diselenite (**I**) or hydrogen selenite (**II**) to the molecular orbitals in certain energy range. Compounds (**I**) and (**II**) exhibit équivalent DOS and PDOS spectra in both configurations (Fig. 14). The energy difference between the consecutive orbitals are generally small. From PDOS (Fig. 14), we note that the occupied orbitals with highest energy are those of the anionic moities $(HSe_2O_5)^-$ and $(HSeO_3)^-$for (**I**) and (**II**) respectively. The lowest energy virtual orbitals are pure adeninium orbitals in both compounds. The interactions between the orbitals of the two entities occur at lower energies. The firsts excited states can be expected to have similar structure to the fondamental state, and feeble energy electronic transitions shall occur without geometric relaxations.

3.3.2. Molecular electrostatic potential (MEP)

The purpose of the studies of molecular electrostatic potential (MEP) surfaces of (**I**) and (**II**) is to resolve the existence of electrostatic interactions between the adeninium cations and hydrogen selenite/diselenite anions based on their charge distribution. The attractive or repulsive nature of electrostatic interactions of (**I**) and (**II**) with other units in crystals can be also identified [67]. The MEP surfaces of the studied compounds (Fig. 15) show that the interaction region between the adeninium cation and the protonated hydrogen diselenite are very attractive in both configurations. The same behavior is observed in both compounds. The regions around the $(HSe_2O_5)^-$ and $(HSeO_3)^-$anions are very attractive toward positive charge. These results are good arguments for the stability of the crystal structure for both compounds.

3.3.3. Mulliken partial charges

The results reported in Table 5 allow to compare the Mulliken partial charges in both compounds. The atoms C6, C8, N6, H6N,

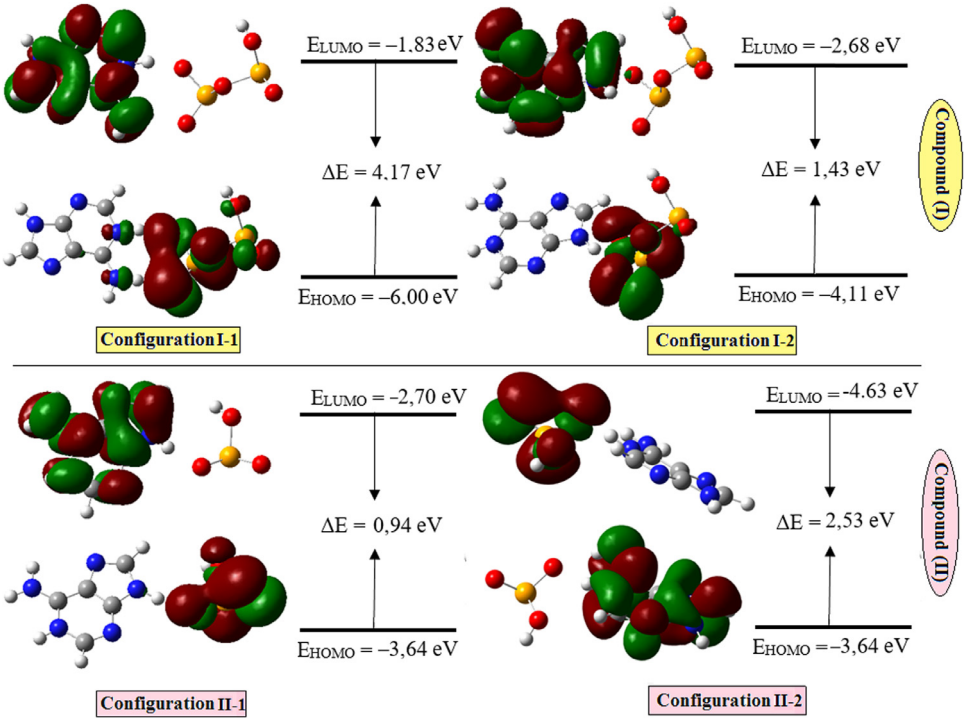

Fig. 13. HOMO and LUMO plots and HOMO-LUMO gaps of configurations **I**-1, **I**-2 and **II**-1, **II**-2 for (**I**) and (**II**) respectively.

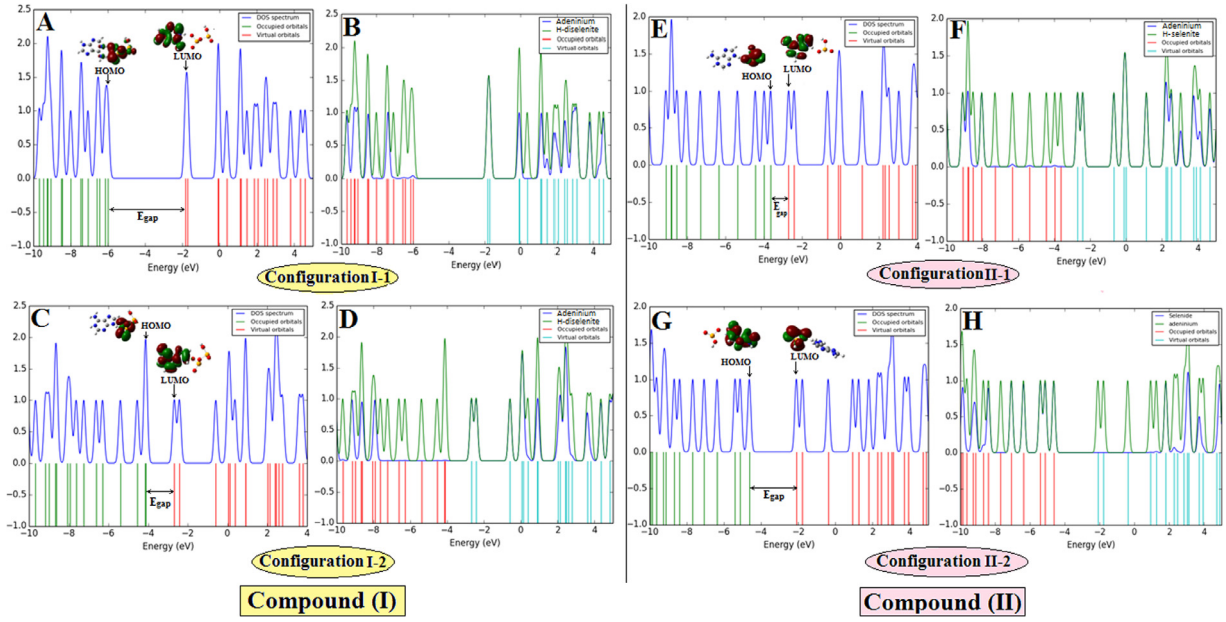

Fig. 14. DOS (**A, C, E** and **G**) and PDOS (**B, D, F** and **H**) spectra of configurations **I**-1, **I**-2 and **II**-1, **II**-2 for (**I**) and (**II**) respectively, and their energy levels of the Frontier Molecular Orbitals.

and H9N exhibit partial charges different by about 0.05e. These differences are attributed, on the one hand, to the adeninium orientation change toward the hydrogen diselenite and hydrogen selenite in (**I**) and (**II**) respectively and, on the other hand, to the difference between the charge distributions of the two anions. The sum of partial charges of adeninium cation is 0.75 (**I-1**), 0.925 (**I-2**), 0.72 (PBC) in (**I**) and 0.827 (**II-1**), 0.79 (**II-2**), 0.799 (PBC) in (**II**). It can be concluded that charge transfer occurs from anions to adeninium cations. This observation is in accordance with the study of protonated nucleobases in their chloride salt crystals which found that the cations are not fully ionized [17,60]. This charge transfer is more pronouced when the configuration is more stable and confirmed by results of calculations under periodic boundary conditions.

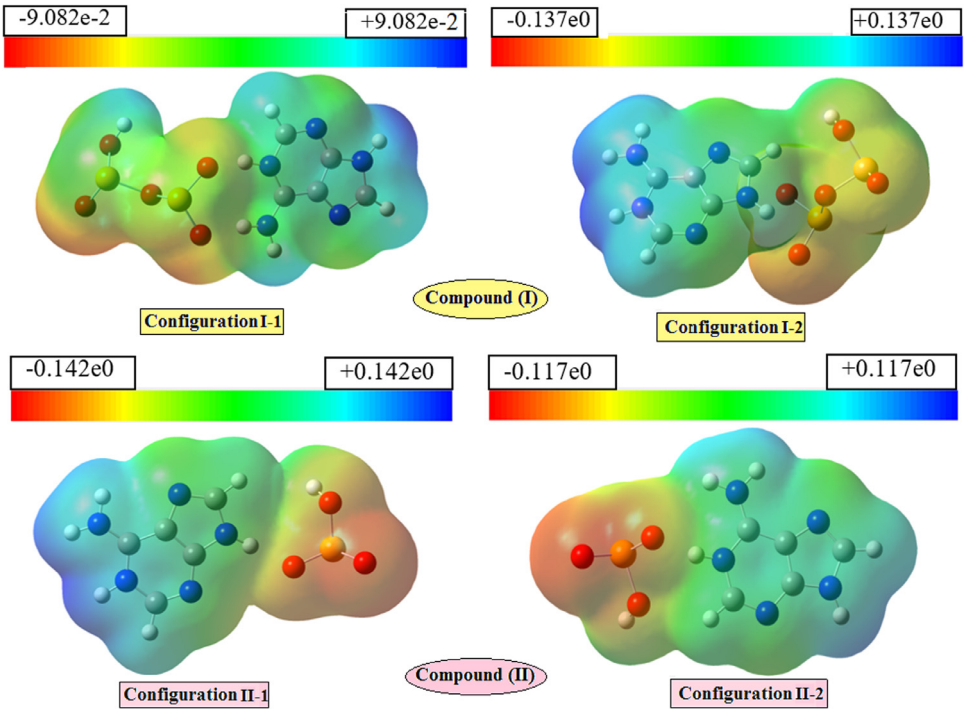

Fig. 15. Molecular electrostatic potential (MEP) of configurations **I**-1, **I**-2 and **II**-1, **II**-2 for (**I**) and (**II**) respectively showing the intermolecular interactions. The isosurface was drawn at 0.0004 e/(Bohr)^3 level of electron density.

Table 5
Mulliken atomic partial charges in **(I)** and **(II)**.

	(I)			(II)		
	Config. I-1	Config. I-2	PBC	Config. II-1	Config. II-2	PBC
1 Se	1021	1022	1042	–	–	–
2 Se	0,988	0,872	1017	0,875	0,888	0,904
3 O	−0,557	−0,576	−0,611	−0,704	−0,631	−0,664
4 O	−0,661	−0,672	−0,685	−0,592	−0,617	−0,610
5 O	−0,594	−0,627	−0,607	−0,660	−0,725	−0,729
6 O	−0,553	−0,576	−0,585	–	–	–
7 O	−0,712	−0,688	−0,663	–	–	–
8 H	0,319	0,318	0,371	0,255	0,294	0,298
9 N	−0,562	−0,581	−0,573	−0,572	−0,555	−0,567
10 N	−0,643	−0,651	−0,665	−0,538	−0,521	−0,545
11 C	0,634	0,651	0,665	−0,652	−0,641	−0,653
12 C	0,201	0,224	0,202	−0,490	−0,542	−0,514
13 N	−0,489	−0,447	−0,490	−0,428	−0,492	−0,487
14 C	0,513	0,540	0,526	0,491	0,495	0,281
15 C	0,276	0,272	0,283	0,277	0,291	0,208
16 N	−0,569	−0,543	−0,579	0,216	0,204	0,618
17 N	−0,495	−0,513	−0,511	0,637	0,632	0,355
18 C	0,292	0,380	0,288	0,302	0,303	0,511
19 H	0,165	0,166	0,192	0,334	0,315	0,314
20 H	0,151	0,173	0,125	0,302	0,325	0,312
21 H	0,331	0,292	0,341	0,299	0,341	0,340
22 H	0,341	0,303	0,341	0,161	0,189	0,163
23 H	0,310	0,333	0,293	0,313	0,301	0,308
24 H	0,294	0,326	0,282	0,175	0,145	0,155

4. Conclusion

To summarize, we have reported in this work, the synthesis, experimental and theoretical characterization of two new adeninium-based organic-inorganic hybrid compounds of formula: $(C_5H_6N_5)^+.(HSe_2O_5)^-$ **(I)** and $(C_5H_6N_5)^+.(HSeO_3)^-$ (**II**). The molecular structures of the studied compounds were determined by single crystal X-ray diffraction study. The atomic arrangement of **(I)** can be described as the succession of cationic layers sandwiched between parallel bilayers of hydrogen diselenite anions developed along the **b**-axis, while in **(II)** the structure is built up from tunnels, prolongated along the **b**-axis. The structural investigation reveals the ability of the 1H,9H adeninium cations to exhibit a variety of hydrogen bonding motifs with hydrogen selenite/diselenite anion. Furthermore, supramolecular homo and hetero-synthons found in (**I**) and (**II**) play an important role in shaping these supramolecular compounds. From the structural comparative study, the stacking interactions present in both com-

pounds were found to be geometrically different. The stacking of organic cations is stabilized in the crystal packing of **(I)** and **(II)** by the ionic bridges with the surrounding anions; this effect should be considered as important in crystal engineering There is an interesting electrostatic association, seen only in compound (**I**), between the SeOH oxygen electron lone pairs and the aromatic cation. In addition, the complementary Hirshfeld surface analysis, enrichment ratios (*E*) and fingerprint plots were used to investigate the relative proportions of intermolecular close contacts existing within the compounds. These analyzes have shown that O···H interactions represent the major contribution of the total Hirshfeld surface in both compounds.

Moreover, HOMO/LUMO energy gaps, MEP surfaces and atomic partial charges have been computed using DFT calculations to get a close insight into the studied compounds. The DFT calculations allowed completing experimental results and show an interesting charge transfer from the inorganic anions to the organic cations.

The results discussed in this work can be useful for investigating the bioactivité process of similar molecular materials through, for example, docking approaches.

Credit author statement

Radhwane Takouachet: Writing, Visualization, Software.

Rim Benali-Cherif: Original draft preparation, Writing, Methodology, Reviewing, Validation**.**

El-Eulmi Bendeif: Writing- Reviewing- Validation.

Christian Jelsch: Hirshfeld surface analysis**,** Writing**,** Reviewing, Validation**.**

Fatima Yahia Cherif: DFT study.

Ali Rahmouni: DFT calculations, Theoritical study, Reviewing, Validation.

Nourredine Benali-Cherif: Structural refinement, Software, Supervision, Reviewing Validation**.**

Appendix A. Supplementary data

CCDC Nº. 1996166 for compound (**I**) and CCDC Nº. 1578761 for compound (**II**) contains the supplementary crystallographic data for this paper. The data can be obtained via www.ccdc.cam.ac.uk/datarequest/cif by e-mailing data_request@ccdc.cam.ac.uk or by contacting the Cambridge Data Cente, 12 Union Road, Cambridge, CB2IEZ, UK

Declaration of Competing Interest

The authors declare that they have no known competing financial interests or personal relationships that could have appeared to influence the work reported in this paper.

Acknowlegments

We gratefully acknowledge the X-ray diffraction platform PMD^{2}X of the Institut Jean Barriol at Université de Lorraine, Pr H. Merazig, Unité de Recherche de Chimie de l'Environnement et Moléculaire Structurale, CHEMS, Université de Constantine, Algeria, and Dr M. Giorgi, Faculté des Sciences et Techniques de Saint Jerôme, Marseille, France, for providing access to the X-ray diffraction facilities. We gratefully acknowledge Pr S. Humbel, CTOM, Aix Marseille Univ, CNRS, Centrale Marseille, iSm2, Marseille, France for providing calculation facilities. We also thank the Algerian MESRS (Ministère de l'Enseignement Supérieur et de la Recherche Scientifique) and DGRSDT (Direction Générale de la Recherche Scientifique et du Développement Technologique) and Abbes Laghrour Khenchela University, for financial support.

Supplementary materials

Supplementary material associated with this article can be found, in the online version, at doi:10.1016/j.molstruc.2020.129836.

References

[1] L.H. Hurley, Nat. Rev. Cancer. 2 (2002) 188–200.
[2] R.P. Verma, C.J. Hansch, Pharm. Sci. 97 (2008) 88–110.
[3] K. Ohara, M. Smeitana, A. Restouin, S. Mollard, J.P. Borg, Y. Collette, J.J. Vasseur, J. Med. Chem. 50 (2007) 6465–6475.
[4] Y.L. Song, Y.L. Li, Z.Y. Wu, J. Inorg. Biochem. 102 (2008) 1691–1699.
[5] H. Cai, S. Su, Y. Li, H. Zeng, Z. Zhu, J. Guo, et al., J. Ethnopharmacol. 212 (2018) 153–165.
[6] G. Roth, G. Moore, W. Kline, T. Poskitt, Transfusion 15 (1975) 116–123.
[7] E.M. Slominska, M. Szolkiewicz, R.T. Smolenski, B. Rutkowski, J. Swierczynski, Nephron 91 (2002) 286–291.
[8] A. Gładysiak, T.N. Nguyen, S.L. Anderson, P.G. Boyd, R.G. Palgrave, J. Bacsa, et al., Inorg. Chem. 57 (2018) 1888–1900.
[9] E.F. Gomez, A.J. Steckl, ACS. Photonics. 2 (2015) 439–445.
[10] M. Irimia-Vladuab, Chem. Soc. Rev. 43 (2014) 588–610.
[11] I. Burneo, K.C. Stylianou, S. Rodríguez-Hermida, J. Juanhuix, X. Fontrodona, I. Imaz, D. Maspoch, Cryst. Growth. Des. 15 (2015) 3182–3189.
[12] R. Benali-Cherif, R. Takouachet, W. Falek, N. Benali-Cherif, C. Jelsch, H. Merazig, M. Hafied, E.-.E. Bendeif, N. Bouslah Mokhnachi, K. Taibi, J. Mol. Struct. 1224 (2021) 129034.
[13] X. Liu, S. Chen, J. Hauser, V. Laukhin, S. Decurtins, U. Aschauer, S.-.X. Liu, Cryst. Growth Des. 16 (2016) 5230–5237.
[14] H. Athmani, C. Kijatkin, R. Benali-Cherif, S. Pillet, D. Schaniel, M. Imlau, N. Benali-Cherif, E.-.E. Bendeif, Acta Cryst A75 (2019) 107–114.
[15] A.- .C.. Marian, D. Nolting, R. Weinkauf, Phys. Chem. Chem. Phys. 7 (2005) 3306–3316 B- Relative energies from density functional theory calculations (taken from ref 17-A):(a) neutral adenine tautomers, 9H (0 kcalmol−1), 7H (7.675 kcalmol−1);(b) protonated adeninium tautomers, 1H,9H (0 kcalmol−1), 3H,7H (0.460 kcalmol−1), 3H,9H (1.971 kcalmol−1), 7H,9H (8.443 kcalmol−1), 1H,7H (10.896 kcalmol−1).
[16] C.R. Groom, I.J. Bruno, M.P. Lightfoot, S.C. Ward, Acta Cryst B72 (2016) 171–179.
[17] P. Kumar, M.K. Cabaj, A. Pazio, P.M. Dominiak, IUCrJ 5 (2018) 449–469.
[18] E. de Matos Gomes, A. Matos Beja, J.A. Paixão, L. Alte da Veiga, M. Ramos Silva, J. Martfn-Gil, F.J. Martin-Gil, Z. Kristallogr. 210 (1995) 929–933.
[19] J.A. Paixão, M. Ramos Silva, A. Matos Beja, E. de Matos Gomes, L. Alte da Veiga, J. Martin-Gil, F.J. Martin-Gil, Z. Kristallogr. 212 (1997) 51–52.
[20] R. Takouachet, R. Benali-Cherif, E.-.E. Bendeif, N. Benali-Cherif, S. Pillet, D. Schaniel, Inorg. Chim. Acta. 446 (2016) 6–12.
[21] L.A. Shulalov, N.R. Ivanov, N.V. Gordeeva, L.F. Kirpichnikova, Soy. Phys. Crystallogr. 14 (1970) 554–558.
[22] Sh.H. Abdel-Hafez, Eur. J. Med. Chem. 43 (2008) 1971–1977.
[23] G. Mugesha, H.B. Singh, Chem. Soc. Rev. 29 (2000) 347–357.
[24] F. Ursini, A. Bindoli, Chem. Phys. Lipids. 44 (1987) 255–276.
[25] R. Takouachet, R. Benali-Cherif, N. Benali-Cherif, Acta Cryst E70 (2014) o186–o187.
[26] R. Benali-Cherif, R. Takouachet, N. Benali-Cherif, Corrélations Structures Propriétés ONL De 3 Nouveaux Composés hybrides: Compréhension des Propriétés Optiques Non Linéaires à Travers La Structure tridimensionnelle. (French Edition) (French) Paperback, Éditions universitaires européennes, May 5, 2017 **ISBN-10**: 3330870141.
[27] M.C. Burla, R. Caliandro, B. Carrozzini, G.L. Cascarano, C. Cuocci, C. Giacovazzo, M. Mallamo, A. Mazzone, G. Polidori, J. Appl. Cryst. 48 (2015) 306–309.
[28] G.M. Sheldrick, Crystal structure refinement with SHELXL, Acta Cryst. C71 (2015) 3–8.
[29] L.J. Farrugia, J. Appl. Crystallogr. 45 (2012) 849–854.
[30] C.F. Macrae, I.J. Bruno, J.A. Chisholm, P.R. Edgington, P. McCabe, E. Pidcock, L. Rodriguez-Monge, R. Taylor, J. van de Streek, P.A. Wood, J. Appl. Cryst. 41 (2008) 466–470.
[31] N. Walker, D. Stuart, Acta. Cryst. A39 (1983) 158–166.
[32] M.A. Spackman, D. Jayatilaka, Hirshfeld Surface Analysis, CrystEngComm 11 (2009) 19–32.
[33] B. Guillot, E. Enrique, L. Huder, C. Jelsch, Acta Cryst A70 (2014) C279.
[34] A.D. Becke, J. Chem. Phys. 98 (1993) 5648–5652.
[35] D. Jacquemin, J. Preat, M. Charlot, V. Wathelet, J.-.M. André, E.A. Perpète, J. Chem. Phys. 121 (2004) 1736–1743.
[36] T.J. Ajayi, M. Shapi, Solvent-free mechanochemical synthesis, hirshfeld surface analysis, crystal structure, spectroscopic characterization and NBO analysis of Bis (ammonium) Bis ((4-methoxyphenyl) phosphonodithioato)-nickel (II) dihydrate with DFT studies, J. Mol. Struct. 1202 (2020) 127254.
[37] S. Brahim, H. Brahim, S. Humbel, A. Rahmouni, Computational studies of Ni (II) photosensitizers complexes containing 1, 1′-bis (diphenylphosphino) ferrocene and dithio ligands, Can. J. Chem. 98 (4) (2020) 194–203.
[38] M.J. Frisch, G.W. Trucks, H.B. Schlegel, G.E. Scuseria, M.A. Robb, J.R. Cheeseman, G. Scalmani, V. Barone, B. Mennucci, G.A. Petersson, H. Nakatsuji, M. Caricato, X. Li, H.P. Hratchian, A.F. Izmaylov, J. Bloino, G. Zheng, J.L. Sonnenberg, M. Hada, M. Ehara, K. Toyota, R. Fukuda, J. Hasegawa, M. Ishida, T. Nakajima, Y. Honda, O. Kitao, H. Nakai, T. Vreven, J.A. Montgomery, Jr., J.E. Peralta, F. Ogliaro, M. Bearpark, J.J. Heyd, E. Brothers, K.N. Kudin, V.N. Staroverov, R. Kobayashi, J. Normand, K. Raghavachari, A. Rendell, J.C. Burant, S.S. Iyengar, J. Tomasi, M.

Cossi, N. Rega, J.M. Millam, M. Klene, J.E. Knox, J.B. Cross, V. Bakken, C. Adamo, J. Jaramillo, R. Gomperts, R.E. Stratmann, O. Yazyev, A.J. Austin, R. Cammi, C. Pomelli, J.W. Ochterski, R.L. Martin, K. Morokuma, V.G. Zakrzewski, G.A. Voth, P. Salvador, J.J. Dannenberg, S. Dapprich, A.D. Daniels, Ö. Farkas, J.B. Foresman, J.V. Ortiz, J. Cioslowski, and D.J. Fox, Gaussian 09, Revision A.02, Gaussian, Inc., Wallingford CT, 2009.
[39] R.D. Dennington, T.A. Keith, J.M. Millam, GaussView 5.0.8, Gaussian Inc., Wallingford, CT, 2008.
[40] N.M. O'Boyle, A.L. Tenderholt, K.M. Langner, J. Comp. Chem. 29 (2008) 839–845.
[41] D. Voet, A. Rich, *Prog.* Nucleic Acid Res. Mol. Biol. 10 (1970) 183–265.
[42] S. Raghunathan, V. Pattabhi, Acta Cryst B37 (1981) 1670–1673.
[43] S. Raghunathan, B.K. Sinha, V. Pattabhi, E.J. Gabe, Acta Cryst. C39 (1983) 1545–1547.
[44] J.P. García-Terán, O. Castillo, A. Luque, U. Garciá-Couceiro, P. Román, F. Lloret, Inorg. Chem. 43 (2004) 5761–5770.
[45] Y. Bo, K. Cheng, S. Bi, S.S. Zhang, Acta Cryst. E62 (2006) o4174–o4175.
[46] J.S. Nirmalram, D. Tamilselvi, P.T. Muthiah, Chem. Crystallogr. 41 (2011) 864–867.
[47] D. Tamilselvi, P.T. Muthiah, Acta Cryst. C67 (2011) o192–o194.
[48] B. Sridhar, K. Ravikumar, B. Varghese, Acta Cryst. C65 (2009) 202–206.
[49] J. Bernstein, R.E. Davis, L. Shimoni, N.-.L. Chang, Angew. Chem. Int. Ed. 34 (1995) 1555–1573.
[50] R. Belhouas, S. Bouacida, C. Boudaren, J.-.C. Daran, E.H. Chtoun, Acta Cryst. E71 (2015) o72–o73.
[51] S. Sedghiniya, J. Soleimannejad, Z. Jahani, J. Davoodi, J. Janczak, Acta Cryst. B76 (2020) 85–92.
[52] L.J. Thompson, N. Elias, L. Male, M. Tremayne, Cryst. Growth Des. 13 (2013) 1464–1472.
[53] B. Sridhar, K. Ravikumar, B. Varghese, Acta Cryst. C70 (2014) 67–74.
[54] E.J.C. de Vries, Sylvia Kantengwa, A. Ayamine, N.B. Bathori, CrystEngComm 18 (2016) 7573–7579.
[55] S. Sedghiniya, J. Soleimannejad, J. Janczak, Acta Cryst. C75 (2019) 412–421.
[56] M. Hadhri, H. Chebbi, A. Haddad, B. Ayed, J. Coord. Chem. 71 (2018) 1035–1047.
[57] R. Takouachet, R. Benali-Cherif, N. Benali-Cherif, Acta Cryst. E70 (2014) o186–o187.
[58] C. Ben Hassen, M. Boujelbene, T. Mhiri, J. Mol. Struct. 1079 (2015) 147–154.
[59] S. Perez-Yanez, O. Castillo, J. Cepeda, J.P. Garcia-Teran, A. Luque, P. Roman, Eur. J. Inorg. Chem. (2009) 3889–3899.
[60] P. Kumar, M.M. Cabaj, P.M. Dominiak, Crystals. 9 (2019) 688–705.
[61] B.E. Hingerty, J.R. Einstein, C.H. Wei, Acta Cryst. B37 (1981) 140–147.
[62] V. Zelenák, Z. Vargová, I. Císarová, Acta Cryst. E60 (2004) o742–o744.
[63] M. Otręba, D. Budzikur, Ł. Górecki, K.A. Ślepokura, Acta Cryst. C 74 (2018) 571–583.
[64] V. Langer, K. Huml, J. Zachová, Acta Cryst. B35 (1979) 1148–1152.
[65] V. Langer, K. Huml, L. Lessinger, Acta Cryst. B34 (1978) 2229–2234.
[66] C. Jelsch, K. Ejsmont, L. Huder, The enrichment ratio of atomic contacts in crystals, an indicator derived from the Hirshfeld surface analysis, IUCrJ 1 (2) (2014) 119–128.
[67] J.M. Seminario, in: Recent Developments and Applications of Modern Density Functional Theory, 4, Elsevier, Amsterdam, 1996, p. 800.